RSC Advances

PAPER

View Article Online
View Journal | View Issue

Cite this: *RSC Adv.*, 2021, **11**, 33399

In situ growth of Fe_3O_4 on montmorillonite surface and its removal of anionic pollutants

Limei Wu, *[a] Jingwen Liu,[a] Yan Liu,[a] Ritong Huang,[a] Ning Tang,[a] Xiaolong Wang[b] and Ling Hu[c]

Received 20th August 2021
Accepted 29th September 2021

DOI: 10.1039/d1ra06318a

rsc.li/rsc-advances

An environmentally functional material for the efficient removal of anionic pollutants in water was prepared for our study. Montmorillonite (M) was modified by hydrochloric acid (HCl) and cetyltrimethylammonium bromide (CTAB). Fe_3O_4 was grown *in situ* to prepare modified Fe_3O_4/montmorillonite (AC Fe_3O_4–Mt) composites. The number of hydroxyl sites on the surface of Mt and the surface tension were increased by HCl and CTAB modification, respectively, which enabled higher Fe_3O_4 surface growth, promoting the multi-directional crystallisation of Fe_3O_4 and improving reactivity. The XRD results show that Fe_3O_4 grows on the surface of Mt and has good crystallinity and high purity, meaning that AC Fe_3O_4–Mt is more reactive than Fe_3O_4. When AC Fe_3O_4–Mt is used to remove anionic pollutants in water, the removal effect under the synergistic action of adsorption-redox is significantly improved, and the maximum removable quantities of Cr(VI) and 2-4-dichlorophenol can reach 41.57 mg g^{-1} and 239.33 mg g^{-1}, respectively. AC Fe_3O_4–Mt is a high efficiency and environmentally functional material with green environmental protection, which can be used in the field of sewage treatment.

1. Introduction

Recent accelerated industrialisation processes have led to a substantial increase in chemical pollutant wastewater discharge. For example, industrial wastewater always contains a large number of pollutants, such as pigments, tanning, electroplating, pesticides, and medicines. Hexavalent chromium ions (Cr(VI)) and 2,4-dichlorophenol (2,4-DCP) are common anionic pollutants from these types of industry.[1,2] They are highly destructive to the environment and toxic to humans. Cr(VI) is the first type of carcinogen[3] which usually exists in aqueous metal–oxygen anion forms, which are strong irritants and carcinogenic if entering the human body. 2,4-DCP causes irritation to human skin and eyes and may damage DNA and induce mutation.[4] Consequently, the United States Environmental Protection Agency had imposed clear regulations on the maximum permissible level of the two pollutants in drinking water. The maximum levels of Cr(VI) and 2,4-DCP in drinking water were set at 0.1 mg L^{-1} [5] and 0.03 mg L^{-1},[6] respectively. Commonly used methods to remove both pollutants include chemically,[7] the Fenton method,[8,9] and an adsorption method.[10,11] As it is operationally simple and easily adaptable, the adsorption method is the most commonly used removal method.

In the traditional adsorption method, the separation process involves membrane filtration and centrifugation, which both increases cost and hinders the large-scale use of adsorption materials.[12] As a type of magnetic nanomaterial, Fe_3O_4 has strong reducibility and recyclability, and can improve pollutant removal efficiency. Montmorillonite (Mt) is a type of clay mineral with a 2 : 1 layered structure. Its structural layer is composed of upper and lower silicon–oxygen tetrahedral layers and intermediate alumina octahedral layers.[13] Due to isomorphous replacement (for example, the Al^{3+} of the octahedral layer being replaced by Mg^{2+} or Fe^{2+}, and the Si^{4+} of the tetrahedral layer being replaced by Al^{3+} or Fe^{3+}), the number and variety of hydroxyl groups on the surface will increase. This drives stronger interactions between Mt and other materials,[14] and it can therefore be used as a good carrier to improve the stability of composites.[15–17] In this study, when Mt is used as a carrier to support Fe_3O_4, due to the large amount of hydroxyl groups on the Mt surface, the unidirectional crystallisation of Fe_3O_4 can be inhibited to form multi-directional crystallisation, and thus improve reactivity. For example, Iñigo Larraza *et al.*[18] reported that magnetite-polyethyleneimine-montmorillonite was used as a magnetic adsorbent to adsorb hexavalent chromium in water. The Mt was subsequently stripped off by the amine group, then the polyethyleneimine-magnetite inserted into Mt layer structure by cation exchange strategy. Finally, the composite was used to adsorb Cr(VI), due to its unique magnetism, demonstrating excellent heavy metal removal capability.

Currently, the common method for inorganic or organic pollutants in water, is to degrade them into non-toxic ions or

[a]School of Materials Science and Engineering, Shenyang Jianzhu University, Shenyang 110168, China. E-mail: lmwu@sjzu.edu.cn; Tel: +86-024-24690315
[b]School of Mechanical Engineering, Shenyang Jianzhu University, Shenyang 110168, China
[c]Planning and Finance Division, Shenyang Jianzhu University, Shenyang 110168, China

adsorb them into material pores.[19,20] In this study, based on the characteristics of rich hydroxyl groups and high Mt surface tension, nano-Fe_3O_4 was grown *in situ*, with Mt as the carrier, to obtain Fe_3O_4–Mt composites. The number and concentration of hydroxyl groups on the Mt surface were increased using acid modification, and the surface tension of Mt was improved by organic modification. Subsequently Fe_3O_4 was crystallised in multiple directions on the Mt surface and the degree of dispersion was simultaneously improved. AC Fe_3O_4–Mt was produced, and the removal efficiency of Cr(VI) and 2,4-DCP was improved. The prepared AC Fe_3O_4–Mt have potentially excellent application prospects for the removal of heavy metals and organic pollutants in water.

2. Materials and methods

2.1 Materials

Ca-based Mt was purchased from Inner Mongolia Ningcheng Tianyu Bentonite Technology Co., Ltd. CTAB was obtained from Tianjin Aopusheng Chemical Co., Ltd. Ferric sulfate ($Fe_2(SO_4)_3 \cdot nH_2O$, $n = 6$–9) was produced by National Pharmaceutical Group Chemical Reagent Co., Ltd. Ferrous sulfate heptahydrate ($FeSO_4 \cdot 7H_2O$) was purchased from Tianjin Beichen Fangzheng Reagent Factory, and sodium hydroxide (NaOH) was purchased from Tianjin Aopusheng Chemical Co., Ltd. All the reagents used are analytical grade and can be used without further purification.

2.2 Preparation of AC Mt

The basic steps to prepare modified Mt are as follows: firstly, 5 g Mt was put into 100 ml HCl solution of 0.5 mol L^{-1} and stirred for 4 hours. Acid-modified polyhydroxy-Mt was then prepared by centrifugally washing with distilled water three times. Next, CTAB with 100%CEC Ca-based Mt exchange capacity, was added to 100 ml distilled water, and acid-modified Mt was added after stirring uniformly. The cation exchange reaction was complete after stirring for 24 hours. Excess CTAB was removed by centrifugal washing until Br ions in the solution can no longer be detected using silver nitrate solution.

2.3 Preparation of AC Fe_3O_4–Mt

Next, an appropriate amounts of ferric and ferrous sulphates were dissolved in distilled water, stirred until a clear, brownish-red solution was obtained. Then enough modified Mt was added to the solution to load 1 g Fe_3O_4, stirred evenly before adding 0.1 mol L^{-1} NaOH buffer solution to pH 12–13. After static ageing for 24 hours, centrifugally wash to neutral, and freeze-dry. Finally, the AC Fe_3O_4–Mt was obtained.

2.4 Material characterization

X-ray diffraction analysis (XRD). The experimental samples were scanned and analyzed randomly by powder loading in the range of 4 °to 70 °under the Cu-Kx radiation generated by 40 mA and 40 kV using Rigaku Ultima IV high-speed array detector.

Specific surface area and pore size analysis (BET). The specific surface area and pore volume of the experimental samples before and after modification were measured by Micromeritics ASAP 2020 specific surface area and a pore size analyzer.

Fourier transform infrared spectroscopy (FT-IR). The FT-IR test of the composites before and after degradation was carried out by using a Thermo Scientific Nicolet iS 5 FTIR spectrophotometer in transmission mode.

Scanning electron microscope (SEM). The Hitachi SU-8020 cold field emission scanning electron microscope combined with the Japanese HORIBA EMAXevolution X-Max 80/EX-270 energy dispersive spectroscopy (EDS) in 10 kV accelerating voltage was used to capture the microstructure image and element content of the prepared composite material sample.

High performance liquid chromatography (HPLC). The liquid phase composition of the solution was determined by Japanese Shimadzu LC15 high performance liquid chromatography in 282 nm.

UV-visible diffuse reflectance spectroscopy (UV-Vis DRS). The absorbance was measured at the maximum absorption wavelength of Cr (372 nm) and 2,4-DCP (286 nm). Before testing, calibrate the instrument with distilled water as a blank control. The absorbance concentration standard curve is used to convert the concentration of the sample solution.

2.5 Adsorption experiment

Initially to determine the effect of pollutant concentration on composite adsorption properties, adsorption experiments were carried out on Cr(VI) and 2,4-DCP, with different concentration gradients, placed in conical bottles at 20 °C. The pH of the solution was adjusted to 5–6. The NaOH and HCl 1 mol L^{-1} solutions were used to adjust the pH of the solution to between 2 and 14, to ascertain the effect of pH on the composite adsorption properties. Under different time intervals, adsorption experiments were carried out, and an equilibrium adsorption time was established. The removed amounts of various initial concentration pollutants were measured at 20 °C, 40 °C, and 60 °C, and the thermodynamic parameters were ascertained.

In the experiment, composite dosages of 2 g L^{-1} and 1 g L^{-1} were used for Cr(VI) and 2,4-DCP respectively, and the pollutants in the solution were filtered after adsorption. The concentration of pollutants in the solution was measured by an ultraviolet spectrophotometer absorbance test. The amount of pollutant adsorbate on the composite material can be obtained using the following formula:

$$q_e = \frac{(C_0 - C_e) \times V}{m}$$

whereas C_0 and C_e represent the initial concentration (mg L^{-1}) and equilibrium concentration in the solution at adsorption equilibrium (mg L^{-1}); V means that the solution volume (L); m is the mass (g) of the composite added.

3. Results and discussion

3.1 Preparation and characterization of composites

The phase compositions of Mt and Fe_3O_4–Mt composites were characterised using X-ray diffraction (Fig. 1). In the Fe_3O_4–Mt composite, the layer spacing of Mt decreased from 1.48 nm to 1.28 nm, proving that part of Fe_3O_4 entered the interlayer of Mt.

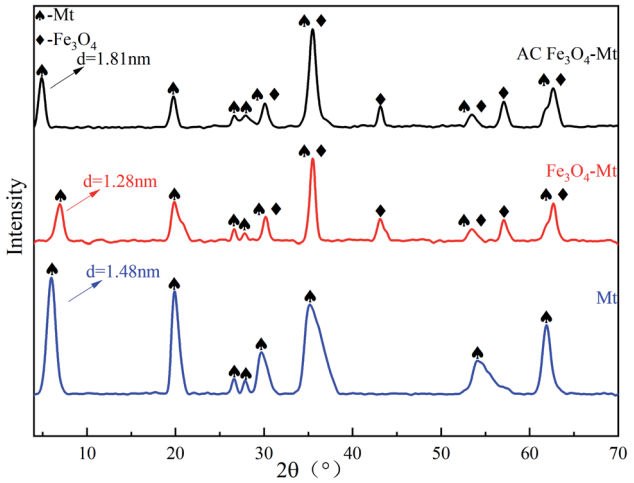

Fig. 1 XRD patterns of Mt, Fe_3O_4–Mt, AC Fe_3O_4–Mt.

The AC Fe_3O_4–Mt characteristic diffraction peak appeared at 2θ = 30.2°, 35.48°, 43.12°, 53.48°, 57.08°, 62.68°of successfully crystallised and grown Fe_3O_4 on AC Mt.[21] The interface of Mt modified by HCl and CTAB also increased visibly, pushing more Fe_3O_4 to load on the Mt surface which was beneficial to the pollutant adsorption process. This verified that AC Fe_3O_4–Mt composites were successfully prepared.

The pore structure properties of Mt, Fe_3O_4–Mt, and AC Fe_3O_4–Mt were analysed by BET specific surface area and BJH pore volume analysis (Fig. 2). The related data were listed in Table 1. The nitrogen desorption experiment produced a type IV isotherm, and the type 2 of the H3 mesoporous hysteresis ring corresponded with the characteristics of a clay mineral layered structure. With the addition of Fe_3O_4, the specific surface area, pore volume, and pore size of the Fe_3O_4–Mt increased to 83 m^2 g^{-1}, 0.21 cm^3 g^{-1}, and 13.70 nm, respectively. This was because Fe_3O_4 was loaded on the Mt surface and a small amount entered the interlayer, resulting in more pores, thus increasing the specific surface area and system pore volume.[22] However, the specific surface area of AC Fe_3O_4–Mt decreased because Fe_3O_4 entered the interlayer and Mt micropores due to CTAB action.[23] According to the pore volume diagram, the micropore structure decreased sharply below 2 nm. The mesoporous and macropores increased greatly over 40 nm, leading to the decrease in pore volume, the rapid decrease in specific surface area, and the increase in average pore size.

The infrared spectra of Mt, Fe_3O_4–Mt, and AC Fe_3O_4–Mt are shown in Fig. 3. 3423 cm^{-1} and 1637 cm^{-1} are Mt interlayer adsorbed water and surface hydroxyl –OH bending vibrations, respectively.[14] There is Si–O tensile vibration at 1032 cm^{-1},[11] Si–O–Al bending vibration, and Si–O–Si bending vibration at 518 cm^{-1} and 463 cm^{-1},[11] respectively. The Si–O tensile vibration, Si–O–Al bending vibration, and Si–O–Si bending vibration of Fe_3O_4–Mt are weakened, and the Fe–O vibration peak at 568 cm^{-1} does not appear, indicating that there is an interaction between Si–O and Fe–O. This facilitates the stable dispersion of Fe_3O_4 on the Mt surface. However, due to the modification of CTAB, the AC Fe_3O_4–Mt exhibits $-CH_2$ symmetrical tensile vibration at 2923 cm^{-1}, $-CH_3$ symmetrical

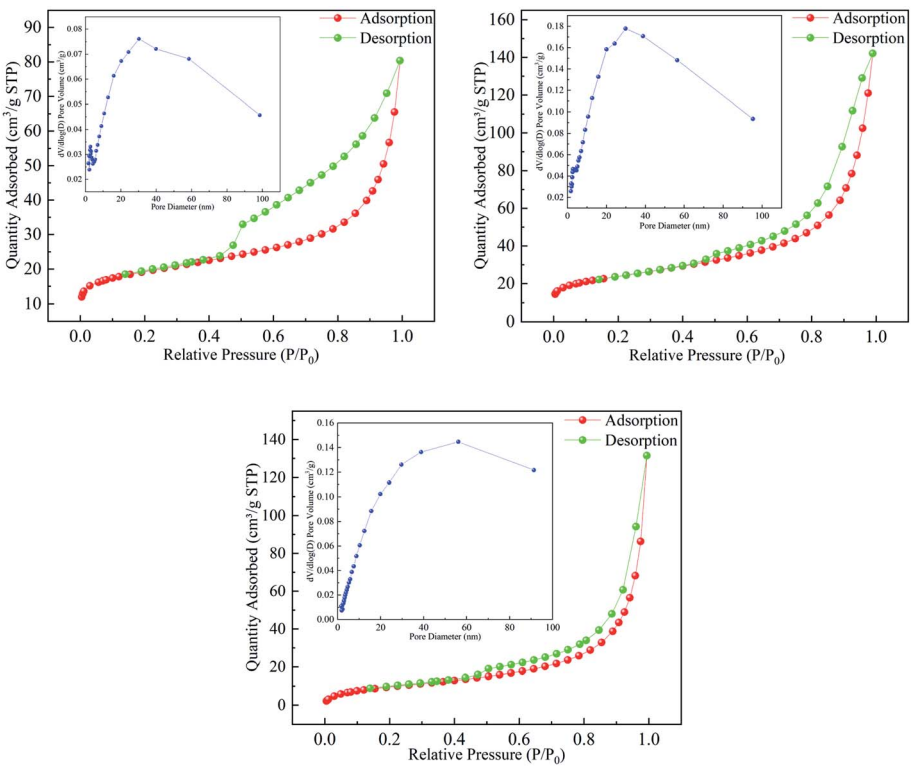

Fig. 2 Nitrogen adsorption–desorption isotherm of Mt, Fe_3O_4–Mt, AC Fe_3O_4–Mt.

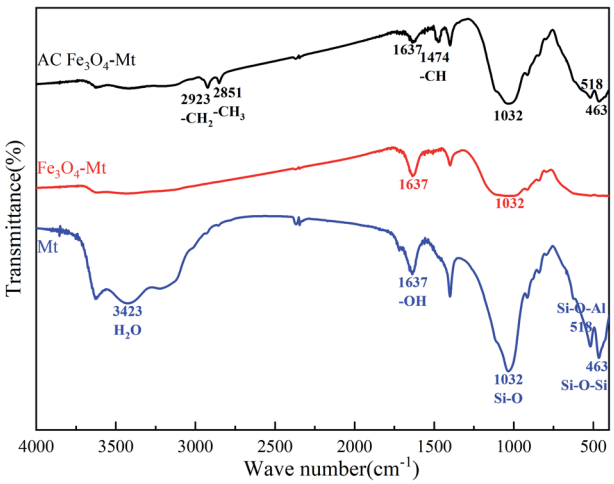

Fig. 3 FT-IR spectra of Mt, Fe_3O_4–Mt, AC Fe_3O_4–Mt.

tensile vibration at 2851 cm^{-1} and –CH deformation vibration at 1474 cm^{-1}.[24]

The surface morphology and element composition of AC Fe_3O_4–Mt were determined by SEM and EDS (Fig. 4). Overall, AC Fe_3O_4–Mt had a layered structure, and nano-sized Fe_3O_4 was uniformly dispersed on the Mt surface. The EDS test results showed that the Fe element content was high, confirming the high loading rate of Fe_3O_4 on Mt.

3.2 Pollutant removal effect of AC Fe_3O_4–Mt

The removal process of anionic pollutants by Mt and Fe_3O_4–Mt composites was affected by solution concentration (Fig. 5a and b). As shown, with an increase of the initial concentration of the solution, the removed amount of Cr(VI) and 2,4-DCP by Mt, Fe_3O_4–Mt, AC Fe_3O_4–Mt increased gradually. This was because the concentration gradient force increased with the increase in initial pollutant concentration, thus augmenting the pollutant diffusion in the solution to the composite, and strengthening its reaction performance.[25] The maximum removable amounts of Cr(VI) by Mt, Fe_3O_4–Mt, and AC Fe_3O_4–Mt were 0 mg g^{-1}, 31.91 mg g^{-1}, and 41.57 mg g^{-1}, respectively, and the maximum removable amounts of 2,4-DCP were 184.81 mg g^{-1}, 158.84 mg g^{-1}, and 239.33 mg, respectively. Compared with Mt and Fe_3O_4–Mt, AC Fe_3O_4–Mt showed stronger removal ability and good stability. The removed amount of Cr(VI) by Mt was zero, in contrast to the higher removal effect of Cr(VI) by Fe_3O_4–Mt. The results showed that Fe_3O_4 in Fe_3O_4–Mt played an important role. The two materials have contrasting effects on the removal of 2,4-DCP with Mt having a much better removal effect. Therefore, Fe_3O_4 in Fe_3O_4–Mt removed pollutants through

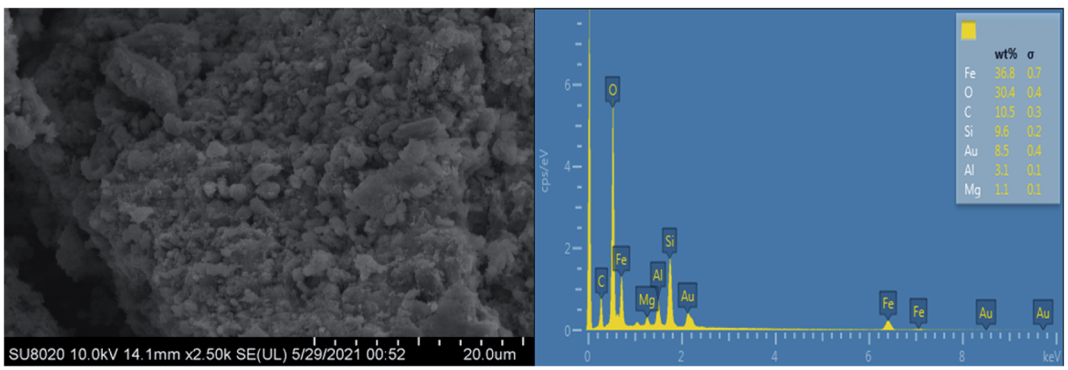

Fig. 4 SEM micrograph and EDS of AC Fe_3O_4–Mt.

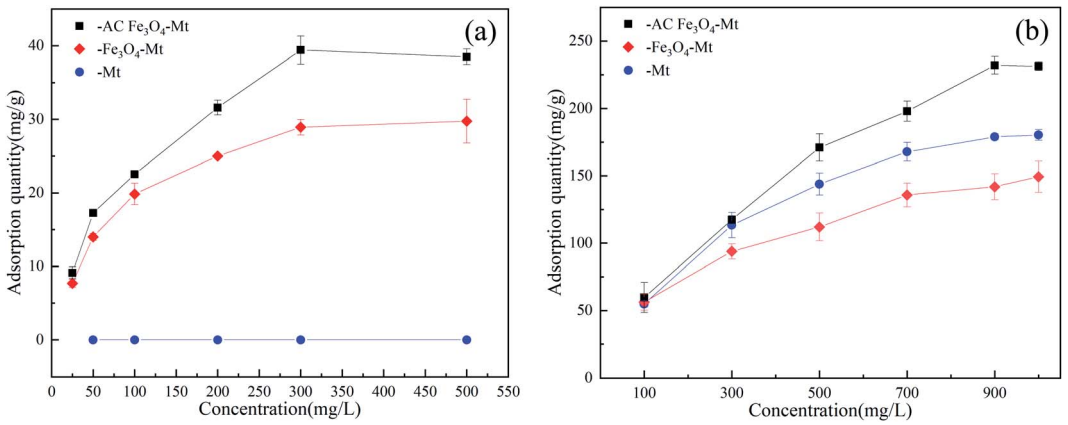

Fig. 5 Effect of initial concentration of Cr(VI) (a) (20 °C, pH = 6), 2,4-DCP(b) (20 °C, pH = 6).

Table 2 Degradation ability of different adsorbents to Cr(VI) and 2,4-DCP

Adsorbents	Q_m (mg g^{-1})	pH	Reference
Cr(VI)			
CPC/Keggin-Al_{30} modified montmorillonite	42.44	2	26
Montmorillonite modified with CTAB and hydroxyaluminum	11.97	4	27
Red mud activated with CTAB	22.20	2	28
Fe–montmorillonite	13.48	4	29
Fe/$Zr_{4:1}$ pillared montmorillonite	22.34	3	30
This study	**41.57**	**6**	
2,4-Dichlorophenol			
Ammonia-modified activated carbon	285.71	6	31
Biocomposites of polypyrrole, polyaniline and sodium alginate with cellulosic biomass	24.57	6	32
Cyclodextrin-ionic liquid polymer	29.58	6	33
Maize cob carbon	17.94	2	34
Pd/Fe–Fe_3O_4@MWCNTs nanohybrids	24.45	6.5	35
This study	**239.33**	**6.5**	

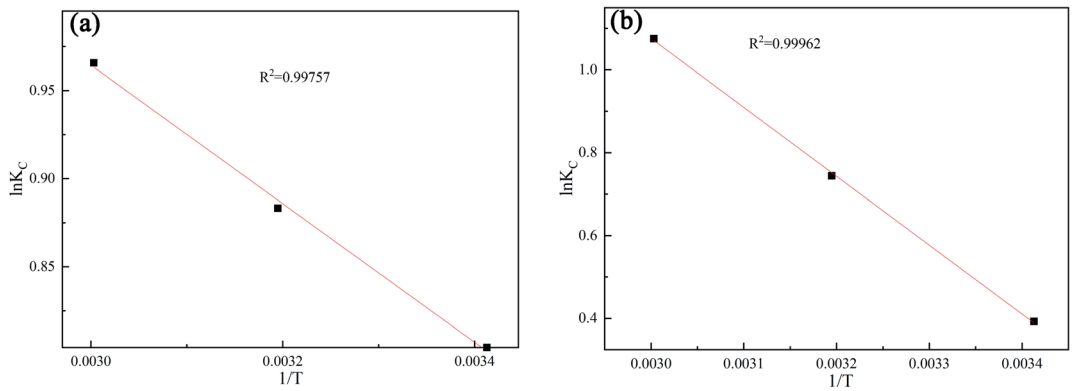

Fig. 6 Plot of ln K_C *vs.* 1/T for estimation of thermodynamic parameters for the adsorption of Cr(VI) (a), 2,4-DCP(b) onto AC Fe_3O_4–Mt. (a) (pH = 6), 2,4-DCP(b) (pH = 6).

redox, which was effective in removing inorganic pollutants, but ineffective at degrading organic ones. Compared with other Mt composites, the AC Fe_3O_4–Mt prepared in this study showed better removal ability of Cr(VI) and 2,4-DCP (Table 2).

The thermodynamic parameters were obtained by using the following equation:

$$K_C = \frac{C_A}{C_S}$$

$$\Delta G = -RT \ln K_C$$

$$\ln K_C = \frac{\Delta S}{R} - \frac{\Delta H}{RT}$$

whereas K_C is the equilibrium constant, ΔS, ΔH and ΔG are the changes of entropy, enthalpy, and Gibbs energy, R is the gas constant, C_S (mg L^{-1}) is the equilibrium concentration and C_A (mg g^{-1}) is the amount of dye adsorbed per unit mass of the adsorbent, and the values of ΔH° and ΔS° were calculated by slope and intercept of plotting ln K_C against 1/T (Fig. 6a and b). The specific parameters were shown in Table 3. The standard Gibbs free energy, ΔG, of Cr(VI) and 2,4-DCP was negative at all test temperatures, indicating that adsorption was spontaneous. The entropy change of the two materials increased slightly, indicating that the structural properties of the composites had

Table 3 AC Fe_3O_4–Mt thermodynamic parameters

Thermodynamic parameters of AC Fe_3O_4–Mt						
	Cr(VI)			2,4-DCP		
T/K	ΔH° (kJ mol^{-1})	ΔS° (J kmol^{-1})	ΔG° (kJ mol^{-1})	ΔH° (kJ mol^{-1})	ΔS° (J kmol^{-1})	ΔG° (kJ mol^{-1})
293	3.2677	17.8216	−1.9592	13.8279	50.4275	−0.9560
313	3.2677	17.8216	−2.2985	13.8279	50.4275	−1.9360
333	3.2677	17.8216	−2.6736	13.8279	50.4275	−2.9757

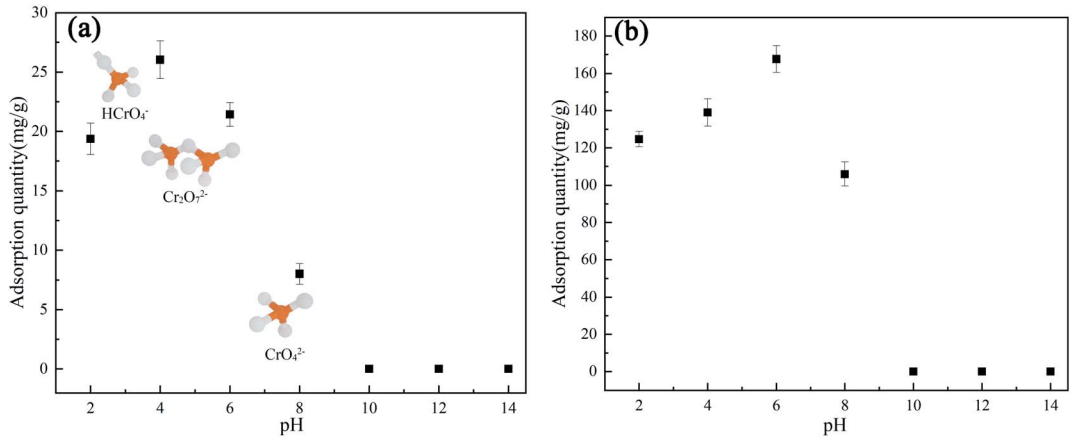

Fig. 7 Effect of pH on AC Fe_3O_4–Mt adsorption of Cr(VI) (a) (20 °C, C_0 = 100 mg L^{-1}), 2,4-DCP(b) (20 °C, C_0 = 500 mg L^{-1}).

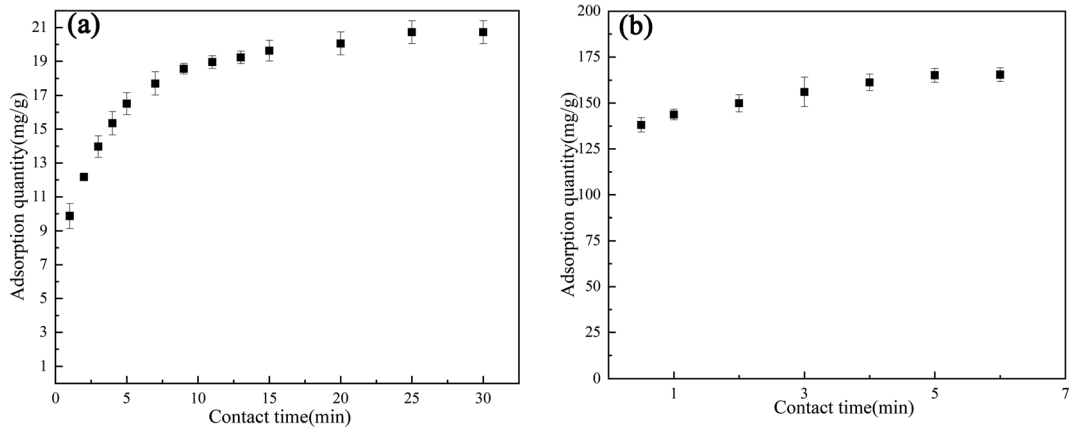

Fig. 8 Effect of contact time on AC Fe_3O_4–Mt adsorption of Cr(VI) (a) (20 °C, pH = 6, C_0 = 100 mg L^{-1}), 2,4-DCP (b) (20 °C, pH = 6, C_0 = 500 mg L^{-1}).

not significantly changed before or after adsorption. The enthalpy change of adsorption of 2,4-DCP was greater than that of Cr(VI). This was due to partial physical adsorption during the degradation of 2,4-DCP,[36] indicating it was highly dependent on temperature. The degradation of Cr(VI) depended mainly on a redox reaction, so the demand for heat was lower, and the temperature effect was only slight.

Additionally, the effect of the solution pH value on the pollutant removal efficiency of AC Fe_3O_4–Mt was established (Fig. 7a and b). In this study, the effect of AC Fe_3O_4–Mt on the removal of Cr(VI) and 2,4-DCP was greatly affected by pH value. The optimum pH value for the removal of 2,4-DCP was 6, while the maximum removed amount of Cr(VI) appeared when the solution pH value was 4. When the pH value of the solution was between 6 to 14, the adsorption capacity of AC Fe_3O_4–Mt to these two pollutants decreases rapidly, and the removed amount was 0 when pH >10. This may be due to the fact that when the solution was alkaline, the large amount of OH^- in the solution competed with the anionic pollutants and occupied a considerable number of adsorption sites, resulting in a decrease in the pollutant adsorption capacity.[37] Because of its weak acidity, lower pH value had little effect on the degradation of 2,4-DCP, but in the degradation of Cr(VI), when the pH value of the solution was 2–6, the main forms of Cr(VI) were $HCrO_4^-$

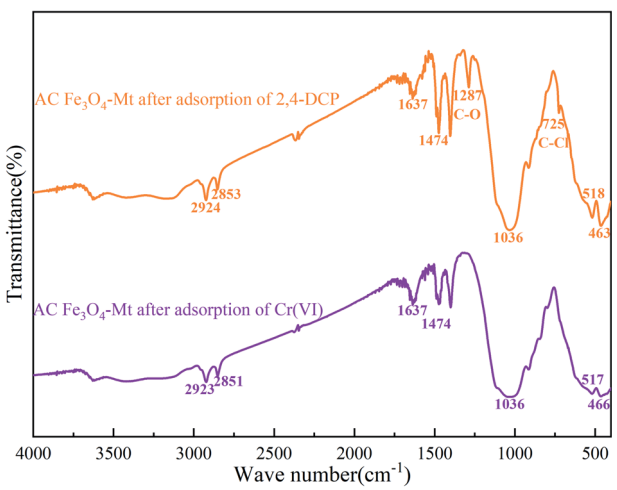

Fig. 9 FT-IR spectra of AC Fe_3O_4–Mt after adsorption.

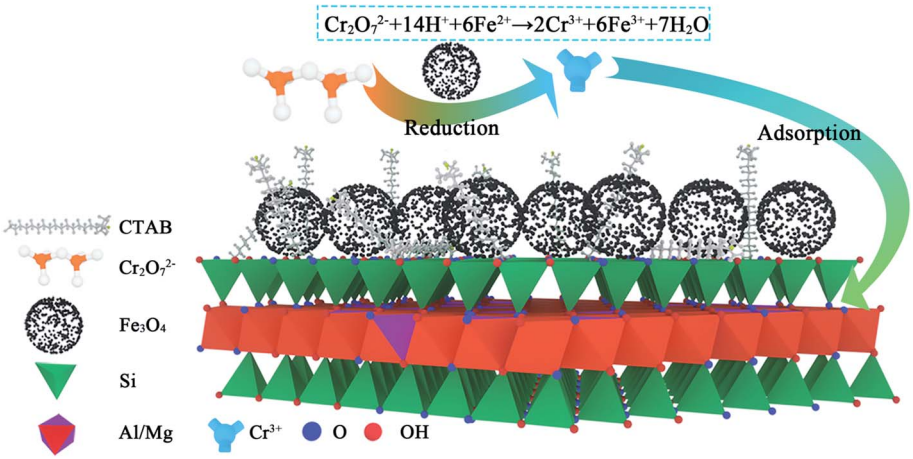

Fig. 10 Mechanism diagram of AC Fe_3O_4–Mt degradation on Cr(VI).

and $Cr_2O_7^{2-}$ ions. When the solution pH >6, there were mainly CrO_4^{2-} ions in the solution,[38] the adsorption sites occupied by the same amount of pollutants increase, and more OH^- in the solution would form competitive adsorption with CrO_4^{2-}. However, when the pH of the solution was less than 2, the removal of Cr(VI) and 2,4-DCP by AC Fe_3O_4–Mt decreased, due to the strongly acidic environment, which destroyed the structure of AC Fe_3O_4–Mt composites then oxidised Fe_3O_4.

Fig. 8 showed that the adsorption capacity of AC Fe_3O_4–Mt to Cr(VI) and 2,4-DCP increased with longer reaction times, and the removal equilibrium was reached at 25 min and 6 min, respectively. The reaction rate was evidently fast. The adsorption of Cr(VI) showed three different adsorption rate trends. In the pre-1 min, there were a large number of reaction sites on AC Fe_3O_4–Mt, and Cr(VI) contacted and reacted with Fe_3O_4 in AC Fe_3O_4–Mt rapidly. Removal also increased rapidly, before the reaction rate slowed down somewhere between 1–10 min. After 10 min, the reaction site was almost saturated, due to the large surface tension of Mt modified by CTAB, physical adsorption was carried out. AC Fe_3O_4–Mt had a faster removal rate of 2,4-DCP, accounting for 81% of the total removal within 30 seconds. Equilibrium was reached at 6 min.

3.3 Analysis of removal mechanism

According to the infrared spectrum of Cr(VI) degraded by AC Fe_3O_4–Mt (Fig. 9), there was no Cr–O vibration peak after the degradation of Cr(VI). This proved that the mechanism of Cr(VI) degradation by AC Fe_3O_4–Mt was not simple adsorption, but that the modified Fe_3O_4–Mt initially reacted with Cr(VI) in solution, and then Cr(VI) ions were adsorbed on the Mt surface. The degradation of Cr(VI) mainly depends on the ability of Fe^{2+} to reduce $Cr_2O_7^{2-}$, and the following reactions took place;

$$Cr_2O_7^{2-} + 14H^+ + 6Fe^{2+} \rightarrow 2Cr^{3+} + 6Fe^{3+} + 7H_2O$$

The specific reaction mechanism was shown in Fig. 10.

In the process of exploring the mechanism of AC Fe_3O_4–Mt's removal of 2,4-DCP, the 2,4-DCP solution before and after removal was determined at 282 nm by high performance liquid chromatography (Fig. 11), to determine whether phenol, 2-CP, and 4-CP were present in the solution after the reaction. Compared with the same concentration of 2,4-DCP solution, there were no phenol, 2-CP, or 4-CP chromatographic peaks before 5 min. Combined with Fig. 9, the characteristic C–O and C–Cl peaks appeared in the removed AC Fe_3O_4–Mt, and there

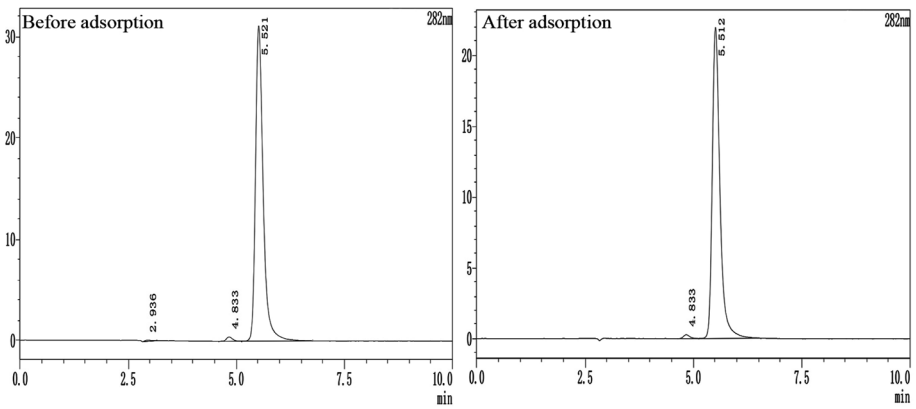

Fig. 11 High performance liquid Chromatography of 2,4-DCP before and after adsorption.

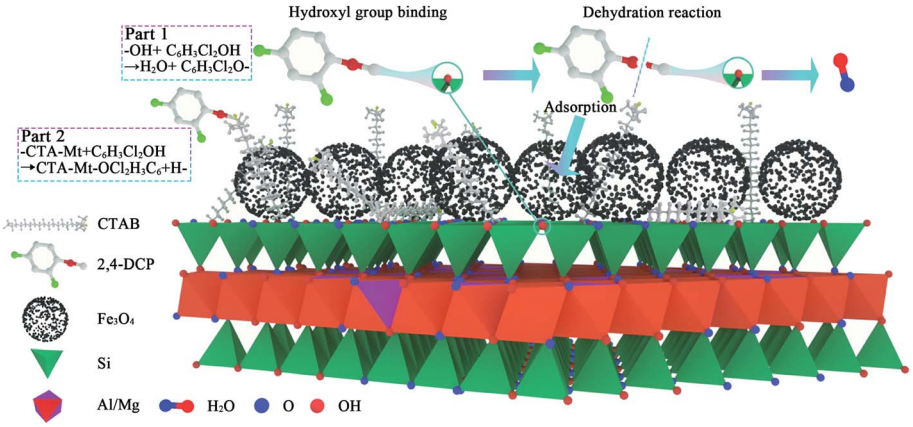

Fig. 12 Mechanism diagram of AC Fe_3O_4–Mt adsorption on 2,4-DCP.

Table 1 Nitrogen adsorption data of Mt, Fe_3O_4–Mt, AC Fe_3O_4–Mt

Samples	Surface area ($m^2\ g^{-1}$)	Pore volume ($cm^3\ g^{-1}$)	Pore size (nm)
Mt	65	0.11	12.06
Fe_3O_4–Mt	83	0.21	13.70
AC Fe_3O_4–Mt	37	0.20	22.05

was no –OH peak, suggesting that there was no de-chlorination reaction, but a dehydration reaction on the hydroxyl group occurred in the 2,4-DCP. According to Liu *et al.*,[39] the strong bond strength of C–Cl was not easily broken. To achieve a de-chlorination reaction, it would be necessary to reduce the pH or use a catalyst.

In summary, the degradation ability of AC Fe_3O_4–Mt on 2,4-DCP is very weak, with the main adsorption occurring during removal. A dehydration reaction occurs between the 2,4-DCP hydroxyl group and the hydroxyl group on the surface of Mt. Subsequently the original Mt hydroxyl site is replaced and adsorption occurs on the Mt surface or interlayer. Furthermore, the combination of 2,4-DCP and Mt loaded CTAB, adsorbs to the Mt surface or interlayer. The specific reaction mechanism is shown in Fig. 12.

4. Conclusions

In this study, a new type of Fe_3O_4–Mt composite material for efficient removal of anionic pollutants was formed. The Mt was modified by HCl and CTAB to increase the number of hydroxyl groups on the Mt surface thus increasing surface tension. This was beneficial in the multi-directional crystallisation of Fe_3O_4 on the surface of Mt and in avoiding agglomeration. Fe_3O_4 was uniformly dispersed on the Mt surface with good crystallinity and high purity, and demonstrated a strong heavy metal and organic pollutant removal performance. The maximum removed amount of Cr(VI) by AC Fe_3O_4–Mt was 41.57 mg g^{-1}, and the maximum removed amount of 2,4-DCP was 239.33 mg g^{-1}, which was both large and reproducible. Additionally, the reaction rate was rapid, and removal equilibrium was reached in 25 min and 6 min, respectively. In addition, the removal effect was also affected by the ambient temperature and pH value of the solution. A higher temperature, and acidic conditions facilitate degradation reactions. AC Fe_3O_4–Mt is a type of environmentally functional material with excellent application potential due to its stable structure and effective heavy metals and organic pollutant removal from water.

Conflicts of interest

There are no conflicts to declare.

Acknowledgements

This research was jointly supported by Liaoning Province "Xingliao Talent Plan Project" (XLYC2007105) and Natural Science Foundation of Liaoning Province (2020-MS-202), and the Research Foundation of Key Laboratory of Deep Geodrilling Technology, Ministry of Natural Resources (No. KF201908).

References

1 A. Baral, R. Engelken, W. Stephens, J. Farris and R. Hannigan, *Arch. Environ. Contam. Toxicol.*, 2006, **50**, 496–502.
2 K. Bentaleb, Z. Bouberka, K. Chinoune, A. Nadim and U. Maschke, *J. Taiwan Inst. Chem. Eng.*, 2017, **80**, 578–588.
3 R. Saha, R. Nandi and B. Saha, *J. Coord. Chem.*, 2011, **64**, 1782–1806.
4 P. Van Aken, R. Van den Broeck, J. Degrève and R. Dewil, *Chem. Eng. J.*, 2015, **280**, 728–736.
5 U. Maheshwari and S. Gupta, *Adsorpt. Sci. Technol.*, 2015, **33**, 71–88.
6 L. Mohammadi, E. Bazrafshan, M. Noroozifar, A. Ansari-Moghaddam, F. Barahuie and D. Balarak, *Water Sci. Technol.*, 2017, **76**, 3054–3068.
7 M. Vinuth, M. Madhukara Naik, K. Karthik, H. S. Bhojya Naik and K. H. Hemakumar, *Res. Chem. Intermed.*, 2019, **45**, 2357–2368.

8 X. Wei, H. Wu, G. He and Y. Guan, *J. Hazard. Mater.*, 2017, **321**, 408–416.
9 L. Xu and J. Wang, *Appl. Catal., B*, 2012, **123–124**, 117–126.
10 J. Shah, M. Rasul Jan, M. Zeeshan and M. Imran, *Appl. Clay Sci.*, 2017, **143**, 227–233.
11 M. Vinuth, H. S. Bhojya Naik and J. Manjanna, *Appl. Surf. Sci.*, 2015, **357**, 1244–1250.
12 H. Ouachtak, R. El Haouti, A. El Guerdaoui, R. Haounati, E. Amaterz, A. A. Addi, F. Akbal and M. L. Taha, *J. Mol. Liq.*, 2020, **309**, 113142.
13 S. Liu, M. Chen, X. Cao, G. Li, D. Zhang, M. Li, N. Meng, J. Yin and B. Yan, *Sep. Purif. Technol.*, 2020, 241.
14 W. S. Jemima, P. Magesan, P. Chiranjeevi and M. J. Umapathy, *Silicon*, 2018, **11**, 925–933.
15 B. S. Kadu, Y. D. Sathe, A. B. Ingle, R. C. Chikate, K. R. Patil and C. V. Rode, *Appl. Catal., B*, 2011, **104**, 407–414.
16 W. J. Dai, P. Wu, D. Liu, J. Hu, Y. Cao, T. Z. Liu, C. P. Okoli, B. Wang and L. Li, *Chemosphere*, 2020, **251**, 126074.
17 S. I. Rathnayake, W. N. Martens, Y. Xi, R. L. Frost and G. A. Ayoko, *J. Colloid Interface Sci.*, 2017, **490**, 163–173.
18 I. Larraza, M. Lopez-Gonzalez, T. Corrales and G. Marcelo, *J. Colloid Interface Sci.*, 2012, **385**, 24–33.
19 I. J. Buerge and S. J. Hug, *Environ. Sci. Technol.*, 1998, **32**, 2092–2099.
20 H. Jia and C. Wang, *Chem. Eng. J.*, 2012, **191**, 202–209.
21 Y. Jin, F. Liu, M. Tong and Y. Hou, *J. Hazard. Mater.*, 2012, **227–228**, 461–468.
22 P. Yuan, M. Fan, D. Yang, H. He, D. Liu, A. Yuan, J. Zhu and T. Chen, *J. Hazard. Mater.*, 2009, **166**, 821–829.
23 J. Yang, K. Yu and C. Liu, *J. Hazard. Mater.*, 2017, **321**, 73–80.
24 Y. Li, Z. Huang, Y. Xia, J. Shi and L. Gao, *Indian J. Chem. Technol.*, 2020, **27**, 116–125.
25 Z. Huang, Y. Li, W. Chen, J. Shi, N. Zhang, X. Wang, Z. Li, L. Gao and Y. Zhang, *Mater. Chem. Phys.*, 2017, **202**, 266–276.
26 X.-y. Zou, F. Xiao, S.-r. Liu, X.-q. Cao, L. Li, M. Chen, L. Dong, X.-j. Lyu and Y.-j. Gai, *Journal of Water Process Engineering*, 2020, **37**, 101348.
27 B. Hu and H. Luo, *Appl. Surf. Sci.*, 2010, **257**, 769–775.
28 D. Li, Y. Ding, L. Li, Z. Chang, Z. Rao and L. Lu, *Environ. Technol.*, 2015, **36**, 1084–1090.
29 L. Ma, Y. Xi, H. He, G. A. Ayoko, R. Zhu and J. Zhu, *Appl. Clay Sci.*, 2016, **120**, 9–15.
30 J. Zhou, P. Wu, Z. Dang, N. Zhu, P. Li, J. Wu and X. Wang, *Chem. Eng. J.*, 2010, **162**, 1035–1044.
31 F. W. Shaarani and B. H. Hameed, *Chem. Eng. J.*, 2011, **169**, 180–185.
32 H. N. Bhatti, Z. Mahmood, A. Kausar, S. M. Yakout, O. H. Shair and M. Iqbal, *Int. J. Biol. Macromol.*, 2020, **153**, 146–157.
33 M. Raoov, S. Mohamad and M. R. Abas, *J. Hazard. Mater.*, 2013, **263**, 501–516.
34 M. Sathishkumar, A. R. Binupriya, D. Kavitha, R. Selvakumar, R. Jayabalan, J. G. Choi and S. E. Yun, *Chem. Eng. J.*, 2009, **147**, 265–271.
35 J. Xu, Z. Cao, X. Liu, H. Zhao, X. Xiao, J. Wu, X. Xu and J. L. Zhou, *J. Hazard. Mater.*, 2016, **317**, 656–666.
36 Y. Fang, A. Zhou, W. Yang, T. Araya, Y. Huang, P. Zhao, D. Johnson, J. Wang and Z. J. Ren, *Sci. Rep.*, 2018, **8**, 229.
37 M. Mobarak, A. Q. Selim, E. A. Mohamed and M. K. Seliem, *J. Mol. Liq.*, 2018, **259**, 384–397.
38 K. Z. Setshedi, M. Bhaumik, S. Songwane, M. S. Onyango and A. Maity, *Chem. Eng. J.*, 2013, **222**, 186–197.
39 H. Liu, X. Ruan, D. Zhao, X. Fan and T. Feng, *Ind. Eng. Chem. Res.*, 2016, **56**, 191–197.